Relaxation of saturated random sequential adsorption packings of discorectangles aligned on a line

Nikolai I. Lebovka [1,*] Mykhailo O. Tatochenko [1,†] Nikolai V. Vygornitskii [1,‡] and Yuri Yu. Tarasevich [2,§]

[1]*Laboratory of Physical Chemistry of Disperse Minerals, F. D. Ovcharenko Institute of Biocolloidal Chemistry, NAS of Ukraine, Kyiv 03142, Ukraine*

[2]*Laboratory of Mathematical Modeling, Astrakhan State University, Astrakhan 414056, Russia*

(Received 19 September 2021; revised 19 November 2021; accepted 22 November 2021; published 6 December 2021)

Relaxation of the packing of elongated particles (discorectangles) aligned on a line was studied numerically. The aspect ratio (length-to-width ratio) for the discorectangles was varied within the range $\varepsilon \in [1; 50]$. The initial jamming (saturated) state was produced using the basic variant of the random sequential adsorption model with random positions and orientations of particles. The relaxation was performed by allowing rotational and translational diffusion motions of the particles while their centers remained located on the line. The effects of the aspect ratio ε on the kinetics of relaxation, the orientation order parameter, and the distribution function of the distances between nearest-neighbor discorectangles were analyzed. The transport properties of the resulting one-dimensional systems were also analyzed by using the diffusion of a tracer particle (random walker) between the nearest-neighbor discorectangles. In the relaxed states the anomalous diffusion was observed having a hopping exponent $d_w > 2$ dependent upon ε.

DOI: 10.1103/PhysRevE.104.064104

I. INTRODUCTION

The problem of one-dimensional (1D) random sequential adsorption (RSA) onto a line (the so-called car parking problem) has been studied in many works in the past [1–6]. In this model, particles of a given shape are placed randomly and sequentially without overlapping any previously placed particles, as their centers are located onto a line. Finally, after a sufficiently long period of deposition ($t \to \infty$), a jamming state is formed such that no additional particles can be added due to the absence of appropriate holes. In the basic variant of RSA, the absence of any relaxation (particle rotations or translations) is assumed.

The problems of assemblies in 1D or quasi-1D systems have also attracted great attention from practical points of view. These assemblies can be useful for the fabrication of photonic and electronic devices, sensors, and biomedical structures [7]. In particular, the microassembly in 1D channels realized by optical tweezers [8], the fabrication of 1D nanoparticle-assembled architectures with excellent optical and electrical performance [9], 1D micro/nanostructures of organic semiconductors for field-effect transistors [10], and 1D micro/nanomotors for biomedicine [11] have been discussed.

The different 1D-RSA problems for particles with arbitrary shapes, e.g., segments (sticks), disks, ellipses, rectangles, discorectangles, etc., have been analyzed [12–14]. For elongated particles, this problem is commonly referred to as the "Paris car parking problem" [15]. For the parking of 1D segments of identical length, the kinetics of the RSA have been described analytically [1,2]. In the jamming state, the following value for the parking coverage (coverage of the line by segments) $\varphi_R = 0.747\,597\,920\,3\ldots$ (Rényi's parking constant) has been obtained [1,16].

Similar problems have been analyzed for modified parking problems where there is the possibility of moving segments [17]; where there are segments of different lengths [18–20]; packing of spins [21]; the presence of arbitrary interaction potentials with finite ranges [22]; where there are "marking street" effects [23]; or psychophysiological packing interactions (involving visual perception of space) [23].

For RSA of particles of a given shape, the jamming coverage depends upon the aspect ratio ε (the length-to-diameter ratio). In particular, for discorectangles it increased from $\varphi = 0.7476$ for $\varepsilon = 1$ (disks), goes through a maximum $\varphi = 0.781\,249 \pm 0.000\,020$) at $\varepsilon \approx 1.5$, and then decreases at higher aspect ratios [14,15]. This nonmonotonic $\varphi(\varepsilon)$ dependence has been explained by the interplay between orientational degrees of freedom and excluded volume effects [12].

The basic variant of the 1D-RSA problem produces out-of-equilibrium systems. By contrast, a diffusionally equilibrated system corresponds to a 1D Tonks gas [24]. The gap distribution functions of totally irreversible and fully equilibrated 1D depositions of line segments demonstrate the presence of strong differences between these two systems [25]. In a modified adsorption-desorption RSA model, the particles can be adsorbed with a rate of k_+, or desorbed with a rate of k_-. The properties of such packings depend on the ratio k_+/k_- [6,26,27]. In such a model, the systems reach equilibrium. However, their kinetics exhibit a succession of regimes before reaching equilibrium. To the best of our knowledge, the

*Corresponding author: lebovka@gmail.com
†tatochenkomihail@gmail.com
‡vygornv@gmail.com
§Corresponding author: tarasevich@asu.edu.ru

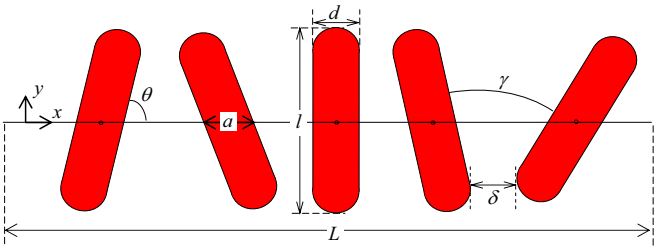

FIG. 1. Schematic picture of the RSA packing of elongated particles onto a line. The particles are hard discorectangles of length l and width d. Intersections of the particles are forbidden. Each deposited particle covers a distance $a(\theta)$ on the line. Periodic boundary conditions are applied along the line (x axis). Here, L is the total length of the line, $\varepsilon = l/d$ is the aspect ratio, θ is the angle between the particle's long axis and the line, and δ and γ are, respectively, the shortest distance and the angle between nearest-neighbor particles.

relaxation of 1D-RSA packings of elongated particles still needs to be studied.

The present paper analyzes, numerically, the relaxation of RSA packings of elongated particles (discorectangles) on a line. The initial state was produced using the basic variant of the 1D-RSA problem [15]. The relaxation was performed while accounting for the rotational and translational diffusion motions of the particles. The rest of the paper is constructed as follows. In Sec. II, the technical details of the simulations are described, all necessary quantities are defined, and some examples of the patterns are presented. Section III presents our principal findings. The transport properties of 1D systems are also analyzed using the diffusion of a tracer particle (random walker) between the elongated particles along the line. Section IV summarizes the main results.

II. COMPUTATIONAL MODEL

The initial state before relaxation was produced using an RSA model [3]. Hard discorectangles (rectangles with a semicircle at each of a pair of opposite sides) with length l and width d were randomly and sequentially deposited onto a line. Overlapping of a particle with any previously deposited ones was forbidden, the orientations of particles were random, and their centers were localized on the line (along the x axis). Each particle has two nearest neighbors from the left and right side on a line (Fig. 1).

A jamming state is where no additional particle can be added to the system due to the absence of any pores of appropriate size. To generate the jamming state a computationally efficient technique based on the tracking of local regions was employed (more detailed information can be found elsewhere [15]). Problems for particles with aspect ratios $\varepsilon \in [1; 50]$ were analyzed. To simplify presentation, all distances were measured in units of particle width. Periodic boundary conditions were used to minimize any finite-size effects. To determine the importance of the system size, a preliminary finite-size scaling analysis for L in the interval $L/\varepsilon \in [4096; 32\,768]$ was performed. Typically, the scaling effects were almost negligible for the length of the line $L/\varepsilon = 2^{15} = 32\,768$ [15], therefore, this value of L was used in all simulations (Fig. 1).

The number density was calculated as $\rho = Nl/L$, where N is the total number of deposited particles. Each deposited particle covers a distance a on the line, thus, the packing coverage was evaluated as $\varphi = \sum_i^N a_i/L$. The orientation of the particles was characterized by the order parameter defined as

$$S = \overline{\cos 2\theta}, \tag{1}$$

where $\overline{\cdots}$ denotes the average over all particles, and θ is the angle between the long axis of the particle and the line (x axis) (Fig. 1). Note that $S = 1$ and $S = -1$ correspond to ideally oriented particles—along the x axis or perpendicular to it, respectively.

The relaxation procedure was performed using the Monte Carlo (MC) approach as follows. At each step, an arbitrary particle was randomly chosen, and its translational and rotation diffusion motions were taken into account.

The translational diffusion coefficients were calculated as [28]

$$D_\parallel = \frac{D_0(\ln\varepsilon + \gamma_\parallel)}{2\pi}, \tag{2a}$$

$$D_\perp = \frac{D_0(\ln\varepsilon + \gamma_\perp)}{4\pi}, \tag{2b}$$

for the motions along and perpendicular to the direction of the long axis, respectively. Here, $D_0 = k_B T/(\eta l)$, $k_B T$ is the thermal energy, and η is the viscosity of the surrounding medium.

The rotational diffusion coefficient was calculated as [28]

$$D_r = \frac{3D_0(\ln\varepsilon + \gamma_r)}{\pi l^2}. \tag{3}$$

In the above Eqs. (3) and (2) the hydrodynamic end-correction factors γ_r, $\gamma_\parallel$, and $\gamma_\perp$ can be evaluated as [28]

$$\gamma_\parallel = -0.207 + 0.980/\varepsilon - 0.133/\varepsilon^2, \tag{4a}$$

$$\gamma_\perp = 0.839 + 0.185/\varepsilon + 0.223/\varepsilon^2, \tag{4b}$$

$$\gamma_r = -0.622 + 0.917/\varepsilon - 0.050/\varepsilon^2. \tag{4c}$$

The centers of the particles were always fixed on the line (x axis). One MC time step ($\Delta t_{MC} = 1$) corresponded to attempted translational displacements along the line and rotations about the center for each of the particles in the system. The amplitudes of the Brownian motions were proportional to the square root of the corresponding diffusion coefficients. The values of these translational Δx and rotational $\Delta\theta$ amplitudes were evaluated using the following equations [29],

$$\Delta x = \sqrt{\Delta r_\parallel^2 + \Delta r_\perp^2} = \beta l \sqrt{1 + \frac{\ln(\varepsilon) + \gamma_\perp}{2[\ln(\varepsilon) + \gamma_\parallel]}}, \tag{5a}$$

$$\Delta\theta = \beta \sqrt{\frac{6[\ln(\varepsilon) + \gamma_r]}{\ln(\varepsilon) + \gamma_\parallel}}. \tag{5b}$$

Here, the value of β was chosen to be small enough ($\beta = 0.02$–0.05) in order to obtain satisfactory acceptance of the MC displacement [30].

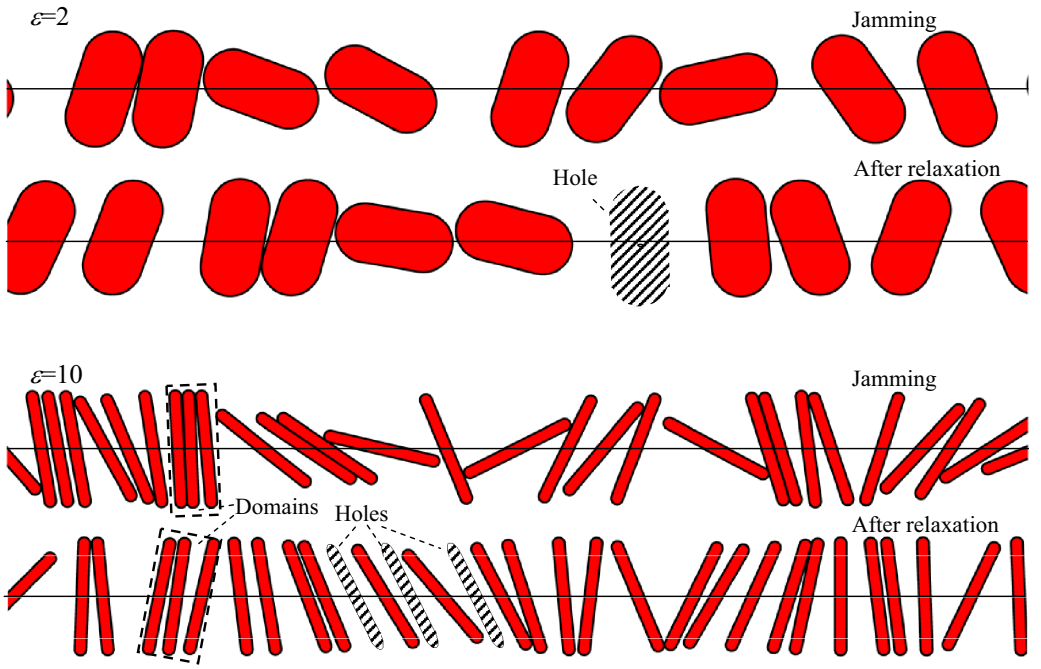

FIG. 2. Examples of the patterns in a jamming state and after complete relaxation for particles with aspect ratios $\varepsilon = 2$ and $\varepsilon = 10$. The relaxation resulted in the appearance of rather large holes (shown as hatched areas). For relatively long particles ($\varepsilon = 10$) domains of nearly parallel particles are also formed.

The Brownian dynamics time increment was evaluated as [31]

$$\Delta t_B = \frac{\mathcal{A}_i}{3}\Delta t_{\rm MC}, \tag{6}$$

where $\mathcal{A}_i$ is the acceptance coefficient for the ith MC step [30], and the total Brownian dynamics time was calculated as

$$t_B = \frac{\Delta t_{\rm MC}}{3}\sum_{i=1}^{t_{\rm MC}}\mathcal{A}_i, \tag{7}$$

where $t_{\rm MC}$ is the MC time.

Time counting was started from the value of $t_{\rm MC} = 1$, being the initial moment (before relaxation), and the total duration required for the complete relaxation of the system in the equilibrium state was typically 10^4-10^5 MC time units (more detailed information can be found elsewhere [29,32]). The completeness of relaxation was controlled by checking the changes in the order parameter S [Eq. (1)].

Figure 2 compares examples of the patterns in the jamming state and after complete relaxation for particles with aspect ratios $\varepsilon = 2$ and $\varepsilon = 10$. Relaxation resulted in the appearance of rather large holes (they are shown as hatched areas) suitable for further packing with new particles. For relatively long particles ($\varepsilon = 10$), domains of nearly parallel particles are also formed both in the jamming state and after complete relaxation. Therefore, the relaxation of RSA packings may result in considerable changes in the structure of such systems.

For each given value of ε, the computer experiments were averaged over 10–100 independent runs. The error bars in the figures correspond to the standard errors of the means. When not shown explicitly, they are of the order of the marker size.

III. RESULTS AND DISCUSSION

Figure 3 shows the order parameter S versus the number density ρ during the RSA process with different values of the aspect ratio ε. At small values of ρ the orientations of the particles were random ($S \approx 0$), while with an increase of ρ, the order parameters decreased and reached their minimum values at the jamming state. This reflected the tendency toward particle ordering perpendicularly to the line, i.e., along the y axis.

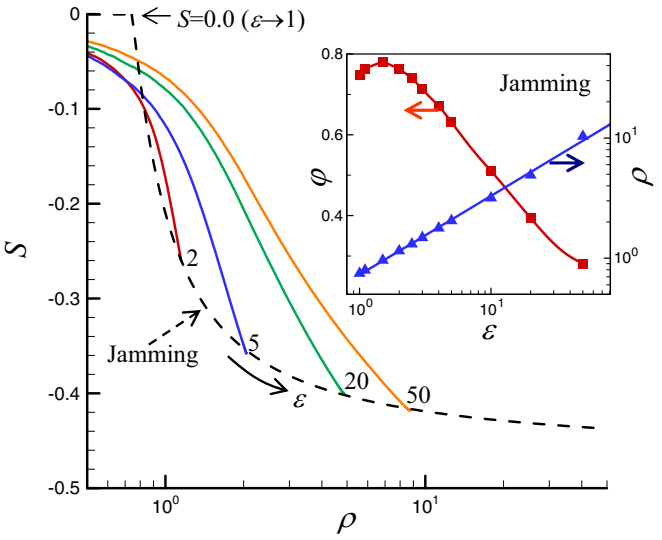

FIG. 3. Order parameter S vs the number density ρ during the RSA process with different values of aspect ratio ε. The dashed line corresponds to the $S(\rho)$ dependence in the jamming state. The inset shows the coverage φ and density ρ of packings in the jamming state vs ε.

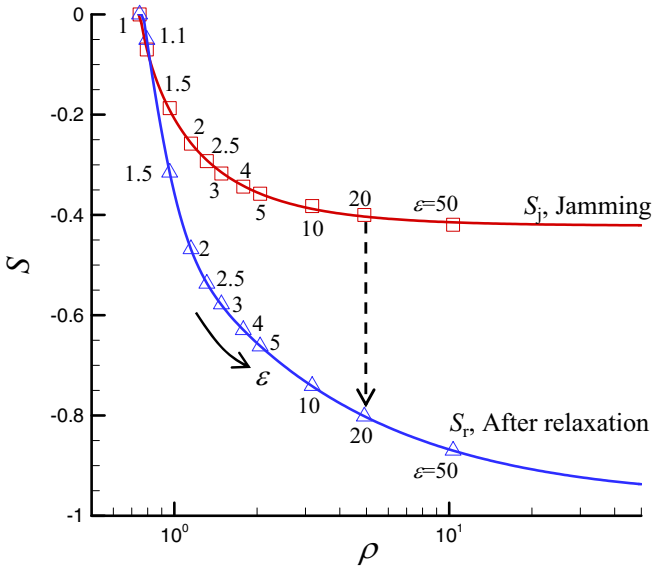

FIG. 4. Order parameter S vs number density ρ in the jamming state and after complete relaxation with different values of aspect ratio ε. In the limit of infinitely thin sticks ($\varepsilon \to \infty$ and $\rho \to \infty$) the order parameter approached the values of $S_j \approx -0.47$ and $S_r \approx -1$ in the jamming state and after complete relaxation, respectively. Here, the symbols correspond to the simulation results, while solid lines are drawn using a Lorentzian cumulative function (see the text for the details).

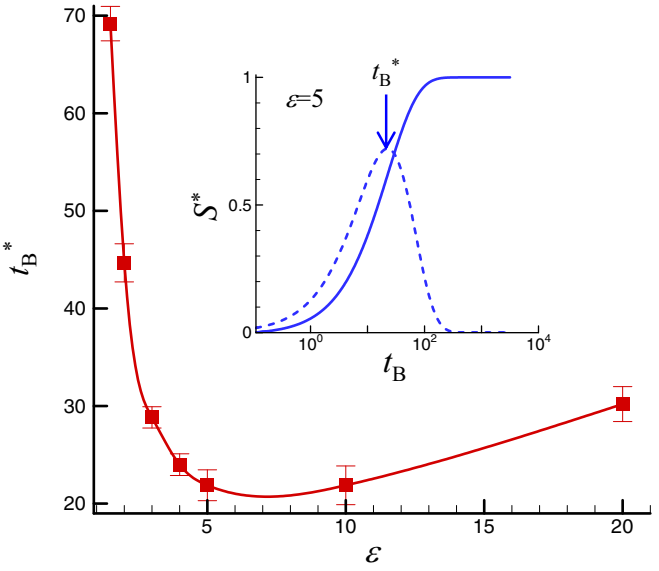

FIG. 5. Characteristic time t_B^* vs the aspect ratio ε. The inset shows an example of a reduced order parameter, $S^* = (S - S_j)/(S_r - S_j)$, vs the Brownian time t_B for the aspect ratio $\varepsilon = 5$ (solid line). Here, the symbols (solid squares) correspond to the simulation results, while a solid line is provided simply as a visual guide. The value of t_B^* was determined from the maximum of the derivative dS^*/dt_B (dashed line). Here, S_j and S_r are the order parameters in the jamming state and after complete relaxation, respectively.

The dashed line shows the $S(\rho)$ dependence in the jamming state. This line was obtained using a Lorentzian cumulative function $S = S_\infty + a(\arctan\{[\log(\rho) - b]/c\} + \pi/2)/\pi$ with parameters $S_\infty = -0.47 \pm 0.01$, $a = 1.67 \pm 0.49$, $b = -0.22 \pm 0.03$, $c = -0.12 \pm 0.02$, and a coefficient of determination $r^2 = 0.9999$. The inset to Fig. 3 compares the coverage $\varphi(\varepsilon)$ and the number density $\rho(\varepsilon)$ dependencies in the jamming state. The well-defined maximum in the $\varphi(\varepsilon)$ dependency ($\varphi = 0.7822 \pm 0.004$ at $\varepsilon \approx 1.46$) can be explained by the competition between the orientational degrees of freedom and the excluded volume effects [12,14,15]. The value ρ grows continuously with ($\rho \approx 0.7476\varepsilon^{0.66}$).

Figure 4 presents the order parameter S vs the number density ρ in both the jamming state (S_j) and after complete relaxation (S_r) with different values of the aspect ratio ε. It is remarkable that, after complete relaxation, the systems had become orientationally ordered. The effects were more pronounced for particles with large values of ε. Particularly, in the limit of infinitely thin sticks ($\varepsilon \to \infty$ and $\rho \to \infty$), the order parameter approached the values of $S_j \approx -0.47$ and $S_r \approx -1$ in the jamming state and after complete relaxation, respectively.

The transition to a more oriented state during relaxation was characterized by changes in the reduced order parameter defined as $S^* = (S - S_j)/(S_r - S_j)$. The value of S^* varied between 0 at $S = S_j$ (jamming state) and 1 at $S = S_r$ (complete relaxation) (solid line in the inset of Fig. 5). To characterize the kinetics of transition from jamming to the complete relaxation state, the characteristic time t_B^* was determined from the maximum in the first derivative curve dS^*/dt_B (dashed line).

Figure 5 presents the characteristic time t_B^* versus the aspect ratio ε. The inset shows an example of the reduced order parameter S^* versus the Brownian time t_B for the aspect ratio $\varepsilon = 5$. The slowest relaxation into the more oriented state was observed for particles with small aspect ratios. For this case, the relaxation has not affected significantly the order parameter (Fig. 4), hence, it is assumed that slow kinetics may reflect translational displacements and the formation of large holes between particles [see Fig. 2(a)]. The value of t_B^* went through a minimum at $\varepsilon \approx 7$. For elongated particles with large values of ε, slow relaxation may be related to the formation of domains of nearly parallel particles (Fig. 2). For this case, the relaxation resulted in significant changes of the order parameter and a transition to the more oriented state (Fig. 4). The observed passing of the t_B^* value through the minimum may reflect competition between the orientational degrees of freedom and the excluded volume effects similar to that observed in the behavior of $\varphi(\varepsilon)$ (Fig. 4). Moreover, it can be also speculated that this extremum reflects the different effects of the particle stacking on the rotational and translational displacements of particles.

Deeper insight into the differences in the systems in the jamming state and after complete relaxation can be obtained by analyzing the distribution functions of the minimum distances $f(\delta)$ [Fig. 6(a)] and angles $f(\gamma)$ [Fig. 6(b)] between nearest-neighbor discorectangles. In the jamming state, the distribution functions of the minimum distances $f(\delta)$ were nonzeros in the interval $0 \leqslant \delta < 1$ and were almost identical for different values of ε. Note that for disks ($\varepsilon = 1$) the obtained function $f(\delta)$ was similar to that observed earlier for the distribution function of the gaps between line segments [25,33].

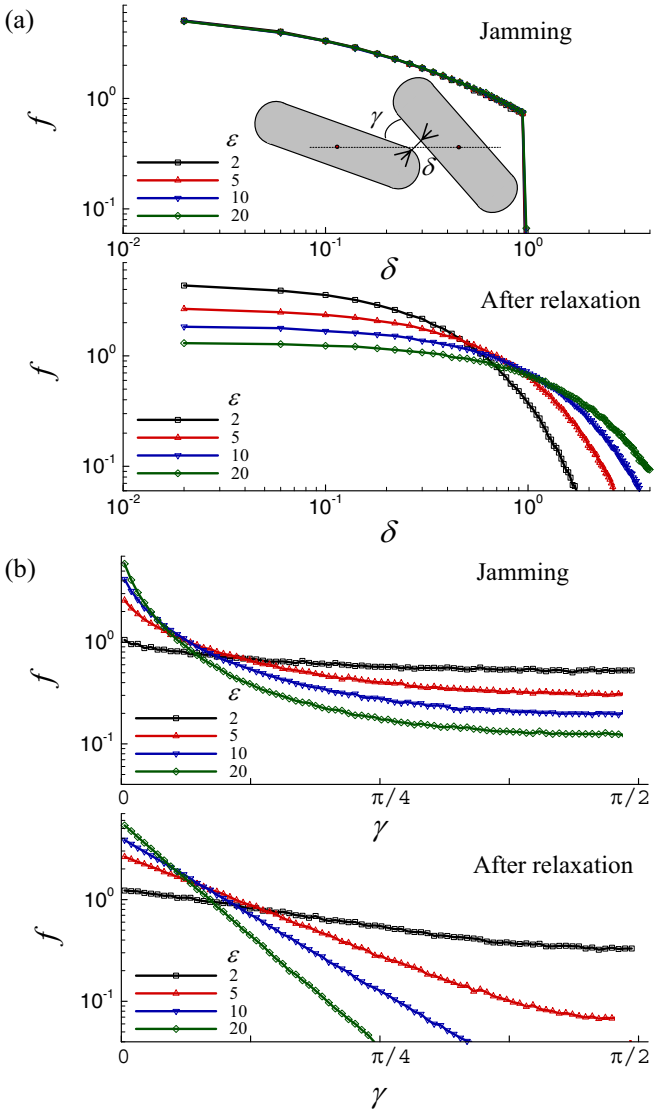

FIG. 6. Distribution functions of the minimum distances $f(\delta)$ (a) and angles $f(\gamma)$ (b) between nearest-neighbor discorectangles with different aspect ratios ε in the jamming state and after complete relaxation.

However, after complete relaxation, the function of $f(\delta)$ changed considerably [Fig. 6(a)]. The values of δ above 1 correspond to the formation of large holes suitable for the deposition of new particles. The effects were more significant for longer particles, with larger values of ε. In particular, the fractions of $f(\delta)$ with δ above 1 constituted $\approx$7.8% and $\approx$50.3% for $\varepsilon = 2$ and for $\varepsilon = 20$, respectively. A significant modification of the distribution functions has also been observed for thermally relaxed line segments (the Tonks gas) [25].

The distribution functions of the angles $f(\gamma)$ between nearest-neighbor discorectangles were descending functions of γ with the maximum located at $\gamma = 0$ [Fig. 6(b)]. Moreover, the values of the function $f(\gamma)$ were dependent on ε, being sharper for longer particles, and the effects were more pronounced for the systems that had undergone complete relaxation [Fig. 6(a)]. The observed effects reflected the

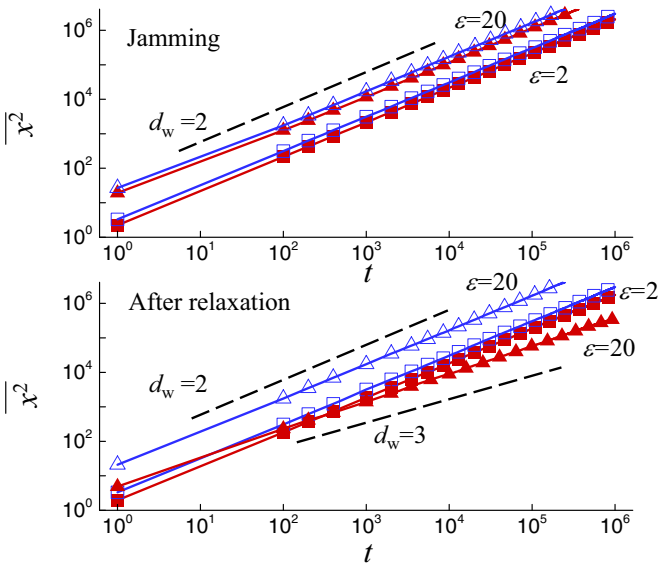

FIG. 7. Mean-square displacement of a tracer particle (random walker) along the line $\overline{x^2}$ vs the time t (number of hopping steps) for systems in the jamming state and after complete relaxation for the aspect ratios $\varepsilon = 2$ (squares) and $\varepsilon = 20$ (triangles). The hopping particle jumps between the nearest-neighbor discorectangles with probability $p = \exp(-\delta/\lambda)$, where δ is the minimum distance between these discorectangles, and λ is a diffusion distance parameter. The data are presented for $\lambda = 1$ (solid symbols) and $\lambda = \infty$ (open symbols). Dashed lines represent the slopes for the hopping exponent $d_w = 2$ and $d_w = 3$.

formation of domains of nearly parallel particles (Fig. 2). This transition to a more oriented state during relaxation was accomplished with a significant sharpening of the function $f(\gamma)$.

Finally, the transport properties of a quasi-one-dimensional system were analyzed using the diffusion of a tracer particle (random walker) between elongated particles along the line [34]. In the model, the point tracer particle performed random jumps (either left or right) to the nearest-neighbor discorectangle with a probability

$$p = \exp(-\delta/\lambda), \tag{8}$$

where λ is a diffusion distance parameter. Note that at $\lambda = \infty$ the jump probability is $p = 1$ and the model is equivalent to unconstrained 1D diffusion. The tracer jumps across the shortest distance δ between discorectangles, and, therefore, diffuses in both the x and y directions. This model assumes a high diffusivity of tracer particles inside the discorectangles and total transport is controlled by the distribution of the distances between nearest-neighbor discorectangles.

In simulations, the mean-square displacement of a tracer particle $\overline{x^2}$ as a function of a discrete time t was analyzed. In the general case, in disordered systems diffusion law can be represented by the following equation [35–39],

$$\overline{x^2} = (t/\tau)^{2/d_w}, \tag{9}$$

where the parameter d_w (the hopping exponent) characterizes the deviation from normal diffusion, and τ is the characteristic diffusion time.

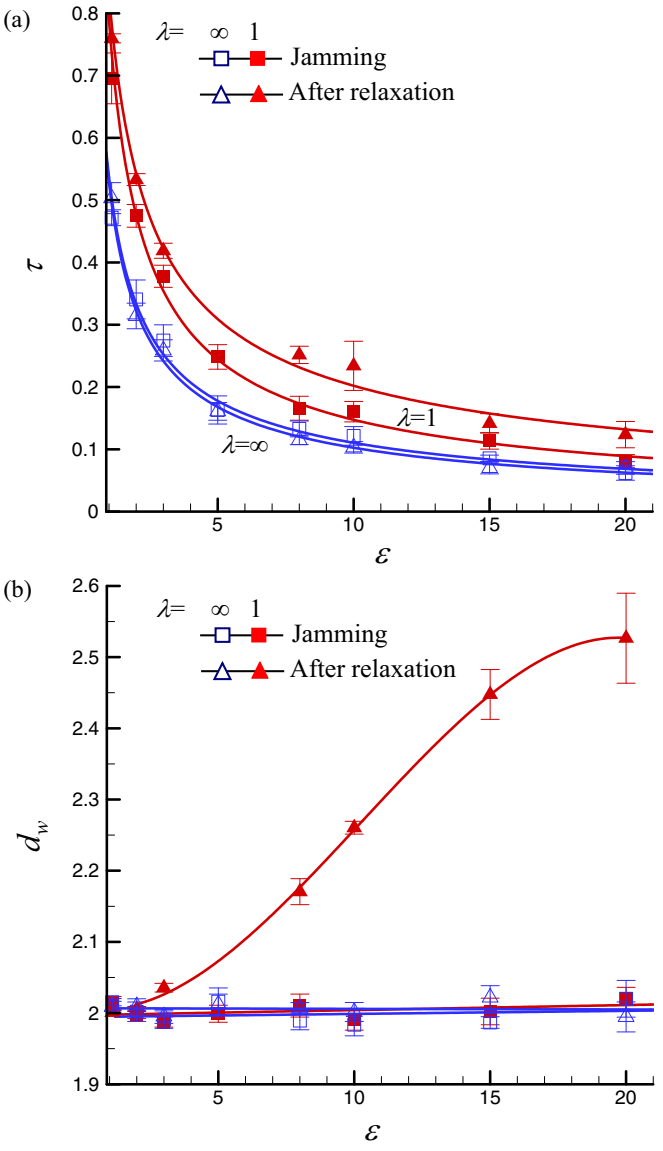

FIG. 8. (a) Characteristic diffusion time τ and (b) hopping exponent d_w vs the aspect ratio ε for systems in the jamming state (squares) and after complete relaxation (triangles) for $\lambda = 1$ (solid symbols) and $\lambda = \infty$ (open symbols). The solid lines are provided simply as a visual guide.

For normal Fickian diffusion, $d_w = 2$, and for 1D systems the diffusion coefficient is $D = (2\tau)^{-1}$. The nontrivial hopping exponent $d_w > 2$ corresponds to the subdiffusion that occurs in disordered systems (e.g., gel-like or fractal) [40].

Figure 7 shows examples of the mean-square displacement of a tracer particle (random walker) along the line $\overline{x^2}$ versus the time t (number of hopping steps) for systems in the jamming state and after complete relaxation. The data are presented for the aspect ratios $\varepsilon = 2$ (squares) and $\varepsilon = 20$ (triangles), and for the diffusion distance parameters $\lambda = 1$ (solid symbols) and $\lambda = \infty$ (open symbols). The dashed lines represent the slopes for the hopping exponent $d_w = 2$ and $d_w = 3$.

No effects of anomalous diffusion were observed for the systems with $\lambda = \infty$, i.e., for normal 1D diffusion. In the jamming state, normal diffusion with the hopping exponent $d_w = 2$ was always observed for all values of ε. However, after complete relaxation, the effects of anomalous diffusion with $d_w > 2$ were evident and could be observed for $\lambda = 1$.

Figure 8 presents examples of the characteristic diffusion time τ [Fig. 8(a)] and the hopping exponent d_w [Fig. 8(b)] versus the aspect ratio ε for systems in the jamming state (squares) and after complete relaxation (triangles) for $\lambda = 1$ (solid symbols) and $\lambda = \infty$ (open symbols). The characteristic diffusion time τ decreased with an increase of ε (Fig. 8). For normal diffusion, it corresponded to the increase of the diffusion coefficient $D = 1/(2\tau)$. This increase of D with ε may reflect the increase in the length of the discorectangles.

A significant increase in the value of the hopping exponent d_w was observed after relaxation. This behavior is in correspondence with the observed effects of relaxation on the distribution functions $f(\delta)$ [Fig. 6(a)].

IV. CONCLUSION

Numerical studies of relaxation packings of elongated particles (discorectangles) on a line were performed. The initial jamming state was produced using the basic variant of the 1D-RSA problem [15]. During the RSA deposition, the orientations of the particles were selected at random. In the RSA state, a tendency towards particle ordering perpendicularly to the line (x axis) was observed. This self-organization was more pronounced for particles with large values of aspect ratio ε. Our findings provide insight into how the value of ε affects the transition from the jamming to the relaxed state. This transition into the more oriented state was accompanied by the formation of domains of nearly parallel particles, and the appearance of rather large holes, suitable for the placement of additional particles. The relaxed systems also demonstrated anomalous transport properties when tested using the diffusion of a tracer particle (random walker).

ACKNOWLEDGMENTS

We acknowledge funding from the National research foundation of Ukraine, Grant No. 2020.02/0138 (M.O.T., N.V.V.), the National Academy of Sciences of Ukraine, Projects No. 7/9/3-f-4-1230-2020, No. 0120U100226, and No. 0120U102372/20-N (N.I.L.), and funding from the Foundation for the Advancement of Theoretical Physics and Mathematics "BASIS," Grant No. 20-1-1-8-1 (Y.Y.T.).

[1] A. Rényi, On a one-dimensional problem concerning random space filling, Select. Transl. Math. Stat. Probab. **4**, 203 (1963) [Magyar Tud. Akad. Mat. Kutató Int. Közl. **3**, 109 (1958)].

[2] J. J. González, P. C. Hemmer, and J. S. Høye, Cooperative effects in random sequential polymer reactions, Chem. Phys. **3**, 228 (1974).

[3] J. W. Evans, Random and cooperative sequential adsorption, Rev. Mod. Phys. **65**, 1281 (1993).

[4] J. Talbot, G. Tarjus, P. R. Van Tassel, and P. Viot, From car parking to protein adsorption: An overview of sequential adsorption processes, Colloids Surf., A **165**, 287 (2000).

[5] S. Torquato and F. H. Stillinger, Jammed hard-particle packings: From Kepler to Bernal and beyond, Rev. Mod. Phys. **82**, 2633 (2010).

[6] P. L. Krapivsky, S. Redner, and E. Ben-Naim, *A Kinetic View of Statistical Physics* (Cambridge University Press, New York, 2010).

[7] O. D. Velev and S. Gupta, Materials fabricated by micro- and nanoparticle assembly—the challenging path from science to engineering, Adv. Mater. **21**, 1897 (2009).

[8] A. Ostendorf, R. Ghadiri, and S. I. Ksouri, Optical tweezers in microassembly, Proc. SPIE **8607**, 86070U (2013).

[9] Y. Li, Z. Zhang, M. Su, Z. Huang, Z. Li, F. Li, Q. Pan, W. Ren, X. Hu, L. Li *et al.*, A general strategy for printing colloidal nanomaterials into one-dimensional micro/nanolines, Nanoscale **10**, 22374 (2018).

[10] Y.-Q. Zheng, J.-Y. Wang, and J. Pei, One-dimensional (1D) micro/nanostructures of organic semiconductors for field-effect transistors, Sci. China Chem. **58**, 937 (2015).

[11] J. Guo and Y. Lin, One-dimensional micro/nanomotors for biomedicine: Delivery, sensing and surgery, Biomater. Transl. **1**, 18 (2020).

[12] P. M. Chaikin, A. Donev, W. Man, F. H. Stillinger, and S. Torquato, Some observations on the random packing of hard ellipsoids, Ind. Eng. Chem. Res. **45**, 6960 (2006).

[13] A. Baule, Shape Universality Classes in the Random Sequential Adsorption of Nonspherical Particles, Phys. Rev. Lett. **119**, 028003 (2017).

[14] M. Cieśla, K. Kozubek, P. Kubala, and A. Baule, Kinetics of random sequential adsorption of two-dimensional shapes on a one-dimensional line, Phys. Rev. E **101**, 042901 (2020).

[15] N. I. Lebovka, M. O. Tatochenko, N. V. Vygornitskii, and Y. Y. Tarasevich, Paris car parking problem for partially oriented discorectangles on a line, Phys. Rev. E **102**, 012128 (2020).

[16] M. P. Clay and N. J. Simányi, Rényi's parking problem revisited, Stoch. Dyn. **16**, 1660006 (2016).

[17] H. Solomon, Random packing density, in *Proceedings of the Fifth Berkeley Symposium on Mathematical Statistics and Probability*, Vol. 5.3 (University of California Press, Berkeley, CA, 1967), pp. 119–134.

[18] S. Anan'evskii, The "parking" problem for segments of different length, J. Math. Sci. **93**, 259 (1999).

[19] M. K. Hassan, J. Schmidt, B. Blasius, and J. Kurths, Jamming and asymptotic behavior in competitive random parking of bidisperse cars, Physica A **315**, 163 (2002).

[20] M. K. Hassan, J. Schmidt, B. Blasius, and J. Kurths, Jamming coverage in competitive random sequential adsorption of a binary mixture, Phys. Rev. E **65**, 045103(R) (2002).

[21] Y. Itoh and L. Shepp, Parking cars with spin but no length, J. Stat. Phys. **97**, 209 (1999).

[22] A. Baule, Optimal Random Deposition of Interacting Particles, Phys. Rev. Lett. **122**, 130602 (2019).

[23] P. Šeba, Parking and the visual perception of space, J. Stat. Mech.: Theory Exp. (2009) L10002.

[24] C. J. Thompson, *Classical Equilibrium Statistical Mechanics* (Clarendon Press/Oxford University Press, New York/Oxford, UK, 1988).

[25] M. R. D'Orsogna and T. Chou, Interparticle gap distributions on one-dimensional lattices, J. Phys. A: Math. Gen. **38**, 531 (2004).

[26] P. Krapivsky and E. Ben-Naim, Collective properties of adsorption–desorption processes, J. Chem. Phys. **100**, 6778 (1994).

[27] P. Viot, Tackling out-of-equilibrium systems by computer simulation: Models of irreversible and reversible adsorption, Eur. J. Phys. **26**, S39 (2005).

[28] H. Löwen, Brownian dynamics of hard spherocylinders, Phys. Rev. E **50**, 1232 (1994).

[29] N. I. Lebovka, N. V. Vygornitskii, and Y. Y. Tarasevich, Relaxation in two-dimensional suspensions of rods as driven by Brownian diffusion, Phys. Rev. E **100**, 042139 (2019).

[30] D. P. Landau and K. Binder, *A Guide to Monte Carlo Simulations in Statistical Physics*, 4th ed. (Cambridge University Press, Cambridge, UK, 2014).

[31] A. Patti and A. Cuetos, Brownian dynamics and dynamic Monte Carlo simulations of isotropic and liquid crystal phases of anisotropic colloidal particles: A comparative study, Phys. Rev. E **86**, 011403 (2012).

[32] N. I. Lebovka, Y. Y. Tarasevich, L. A. Bulavin, V. I. Kovalchuk, and N. V. Vygornitskii, Sedimentation of a suspension of rods: Monte Carlo simulation of a continuous two-dimensional problem, Phys. Rev. E **99**, 052135 (2019).

[33] S. Rawal and G. Rodgers, Modelling the gap size distribution of parked cars, Physica A **346**, 621 (2005).

[34] J. W. Haus and K. W. Kehr, Diffusion in regular and disordered lattices, Phys. Rep. **150**, 263 (1987).

[35] R. Metzler and J. Klafter, The random walk's guide to anomalous diffusion: A fractional dynamics approach, Phys. Rep. **339**, 1 (2000).

[36] S. Havlin and D. Ben-Avraham, Diffusion in disordered media, Adv. Phys. **51**, 187 (2002).

[37] N. Masuda, M. A. Porter, and R. Lambiotte, Random walks and diffusion on networks, Phys. Rep. **716**, 1 (2017).

[38] F. A. Oliveira, R. Ferreira, L. C. Lapas, and M. H. Vainstein, Anomalous diffusion: A basic mechanism for the evolution of inhomogeneous systems, Front. Phys. **7**, 18 (2019).

[39] M. A. dos Santos, Analytic approaches of the anomalous diffusion: A review, Chaos Solitons Fractals **124**, 86 (2019).

[40] P. Kubala, M. Cieśla, and B. Dybiec, Diffusion in crowded environments: Trapped by the drift, Phys. Rev. E **104**, 044127 (2021).